RESEARCH ARTICLE

ADVANCED OPTICAL MATERIALS
www.advopticalmat.de

Overcoming the Short-Wave Infrared Barrier in the Photoluminescence of Amino-As-Based InAs Quantum Dots

Satyaprakash Panda, Dongxu Zhu, Luca Goldoni, Aswin Asaithambi, Rosaria Brescia, Gabriele Saleh, Luca De Trizio, and Liberato Manna**

The synthesis of amino-As-based InAs quantum dots (QDs) with narrow excitonic absorption features and efficient photoluminescence (PL) beyond 1000 nm remains a considerable challenge. A key limitation lies in the use of conventional reducing agents, which typically release low-boiling byproducts. These volatile species cause temperature fluctuations, leading to unstable reaction conditions that are detrimental in seeded growth strategies. In this work, we demonstrate that trioctylamine-alane (TOA-AlH_3), a reducing agent with a high boiling point, enables the one-pot synthesis of InAs QDs with narrow excitonic absorption peaks extending up to 935 nm. Upon ZnSe shell growth, these QDs exhibit high PL quantum yields (QYs) of 75% and 60% at 905 and 1000 nm, respectively, which are record values for amino-As-based InAs@ZnSe systems. Moreover, TOA-AlH_3 is applied in a seeded growth approach to prepare larger InAs QDs, achieving narrow excitonic absorption up to 1350 nm. After ZnSe shelling, these samples exhibit PLQYs of 46%, 38%, 32%, and 23% at 1160, 1250, 1335, and 1430 nm, respectively. Importantly, TOA-AlH_3 is compatible with $ZnCl_2$, a necessary additive for reaching high PLQYs. These advancements establish a robust and scalable synthetic route to highly luminescent InAs QDs, paving the way for their integration into next-generation infrared optoelectronic applications.

1. Introduction

Future consumer markets for infrared (IR) products will require inexpensive and efficient IR-active materials. IR applications of interest include photovoltaics, light-emitting diodes (LEDs), lasers, security/anti-counterfeiting technologies, optical communication, biological imaging, night and fog vision.[1–11] IR colloidal quantum dots (QDs) are ideal candidates to address this challenge, as they can be fabricated using cost-effective wet chemical methods and can be easily integrated using techniques such as inkjet printing onto complementary metal-oxide-semiconductor (CMOS) technologies.[1,4–6,9–13] Indeed, IR QDs have been already implemented in prototype IR devices including lasers, sensors, and LEDs.[1,4–6,8–15]

In this context, the best device performance so far has been achieved with IR QDs based on Pb- and Hg-chalcogenides, whose synthesis strategies are currently well established.[16–19] However, the intrinsic toxicity of these materials makes them unsuitable candidates for the IR consumer market and is driving research toward less toxic alternatives.[20,21] The most promising IR QD compounds compliant with the Restriction of Hazardous Substances (RoHS) directive[22] include Ag- and Cu-based I-III-VI semiconductors (namely $AgInSe_2$, $CuInSe_2$, and $CuInS_2$), InSb, and InAs QDs.[23–27] InAs QDs, thanks to their tunable optical bandgap, which can be adjusted from ≈540 to ≈1700 nm by quantum confinement, are among the most promising candidates for IR applications.[8,14,15,28–39]

Two main colloidal routes are currently employed to synthesize InAs QDs: one is based on tris-trimethylsilyl arsine (TMS-As) and

S. Panda, D. Zhu, A. Asaithambi, G. Saleh, L. Manna
Nanochemistry
Istituto Italiano di Tecnologia
Via Morego 30, Genova 16163, Italy
E-mail: liberato.manna@iit.it

The ORCID identification number(s) for the author(s) of this article can be found under https://doi.org/10.1002/adom.202501512

DOI: 10.1002/adom.202501512

S. Panda
Dipartimento di Chimica e Chimica Industriale
Università di Genova
Genova 16146, Italy

L. Goldoni
Materials Characterization
Istituto Italiano di Tecnologia
Via Morego 30, Genova 16163, Italy

L. De Trizio
Chemistry Facility
Istituto Italiano di Tecnologia
Via Morego 30, Genova 16163, Italy
E-mail: luca.detrizio@iit.it

R. Brescia
Electron Microscopy Facility
Istituto Italiano di Tecnologia
Via Morego 30, Genova 16163, Italy

the other on tris-dimethylamino arsine (amino-As).[32,37,40–48] The former, developed in the late nineties, is the most advanced of the two and has been optimized to prepare InAs QDs with a narrow excitonic absorption peak (indicative of a narrow size distribution), which can be tuned up to 1600 nm. However, this wavelength can only be achieved through a laborious seeded growth approach, and the emission properties/photoluminescence (PL) efficiency of these systems have not yet been investigated.[4,8,34] Due to the high cost, toxicity, and pyrophoricity of the TMS-As precursor, the use of amino-As, a much cheaper and less reactive As precursor, has gained popularity in recent years.[37,39,43–49]

To implement amino-As-based InAs NCs in optoelectronic devices, their optical properties require further optimization, not only in terms of their absorption peak position and linewidth,[33,34,45,50] but also in their PL quantum yield (QY), especially at wavelengths beyond 1000 nm.[35,42,51] Indeed, the synthesis of emissive large amino-As-based InAs QDs, capable of efficient PL at wavelengths beyond 1000 nm, remains a significant challenge. Indeed, while PLQYs as high as 70% have been reported for amino-As-based InAs QDs with emission at ≈950 nm,[39,46,48] no emission or only poor PL efficiencies have been reported for longer wavelengths. For instance, Kim et al. synthesized amino-As-based InAs QDs with absorption extending to 1700 nm via the combined use of diisobutylaluminum hydride (DIBAL-H) as the reducing agent and lithium bis(trimethylsilyl)amide as an additive, but no PL was reported.[38] Leemans et al. developed a synthesis strategy based on amino-P as the reducing agent, which delivers amino-As-based In(As,P) QDs with absorption peak tunable up to 1600 nm; however, no PL efficiency data were reported.[37] More recently, Skorotetcky et al. devised a continuous injection strategy relying on 1,1,3,3,5,5-hexamethyltrisiloxane (HMTS) as the reducing agent, through which they synthesized amino-As-based InAs QDs with absorption tunable up to 1550 nm, but the PL properties were not discussed.[49]

These considerations motivated our current work, in which the primary focus was to achieve amino-As-based InAs QDs emitters with tunable and efficient emission beyond 1000 nm. To reach this goal, we devised a synthesis strategy to InAs@ZnSe QDs with PL extending up to 1400 nm and PLQYs as high as 60% at 1000 nm, 46% at 1160 nm, 38% at 1250 nm, 32% at 1335 nm and 23% at 1430 nm. This was achieved by modifying our recently published synthesis approach for InAs QDs, which uses $ZnCl_2$ as a crucial additive.[39,46,48] The novelty of the present work lies in the introduction of a new reducing agent, trioctylamine alane (TOA-AlH_3), which we synthesized as a replacement for dimethylethylamine alane (DMEA-AlH_3). DMEA-AlH_3 is currently regarded as the most effective reducing agent when paired with amino-As to achieve optimal control over the size distribution of InAs QDs.[45–48] However, the maximum achievable size for InAs QDs is limited to ≈3 nm, corresponding to a PL peaked at most at 950–970 nm.[39,45,46,48] The synthesis of larger InAs QDs with DMEA-AlH_3, via either one-pot procedures or seeded growth approaches, is impeded by the following drawbacks:

1) DMEA-AlH_3 is commercially available only dissolved in low-boiling solvents, such as toluene, hence, when injected into a hot mixture (typically at 240–280 °C), it can cause a boiling burst;
2) upon cleavage of the Al—N bond, which occurs at ≈130 °C,[52] DMEA is released into the reaction mixture, also causing vigorous boiling.

The low boiling points of both the amine (DMEA) and the solvent (toluene) lead to significant temperature fluctuations during the reaction, making it difficult to control the reaction progress and, importantly, produce a considerable amount of vapors in the reaction flask, posing safety risks. We would like to emphasize here that the other reported reducing agents, if used to prepare large amino-As-based InAs QDs, should also suffer from analogous issues: i) DIBAL-H is typically commercially available in solvents such as toluene, hexane, or THF; ii) amino-P and HMTS have boiling points that are much lower (150 and 128 °C, respectively) than the temperatures required for InAs QD synthesis (i.e., 240–280 °C).

As demonstrated in this work, these issues can be effectively addressed using TOA-AlH_3 as the reducing agent. This compound features a reduction kinetics toward As^{3+} species similar to that of DMEA-AlH_3, as they are both aminoalanes: i) the cleavage of the N—Al bond occurs at similar temperature ranges (130–150 °C);[52] ii) the actual reducing agent is AlH_3, which is released upon cleavage of the N—Al bond. However, unlike DMEA-AlH_3, TOA-AlH_3 does not cause any temperature fluctuations or vapor formation during the InAs QDs synthesis, since it readily dissolves in high-boiling non-coordinating solvents, such as octadecene (ODE) or squalane and releases TOA (which has a boiling point of ≈365 °C at 1 atm) upon cleavage of the Al—N bond. We first demonstrated that TOA-AlH_3 can be successfully employed in the one-pot hot-injection synthesis of amino-As-based InAs QDs, delivering QDs with a very narrow absorption peak (half-width at half-maximum, HWHM, as low as 85 meV, which is among the lowest values reported for amino-As based systems)[44,45,47–50] and tunable up to 935 nm. Upon growth of a ZnSe shell on top of these QDs, we obtained InAs@ZnSe core@shell QDs with a PLQY as high as 75%, with emission at 900 nm, comparable to state-of-the-art values, and 60% for systems with PL peaking at 1000 nm, a record value.

Leveraging on the efficiency of our new reducing agent, we then devised a seeded-growth approach to further enlarge the InAs QDs. Our experiments indicated that the optimal procedure to achieve this goal involves the injection of $InCl_3$ into the crude InAs QD reaction solution, followed by the simultaneous co-injection of TOA-AlH_3 and amino-As at 240 °C. This approach enabled the preparation of InAs QDs with absorption tunable up to 1340 nm. ZnSe shelling of these QDs resulted in InAs@ZnSe core@shell structures with PLQY values as high as 46% (PL at 1160 nm), 38% (PL at 1250 nm), 32% (PL at 1335 nm), and 23% (PL at 1430 nm) which are record values with the amino-As route. It is worth highlighting that such high PL efficiencies were observed only when $ZnCl_2$ was employed in the synthesis of InAs QDs. Indeed, when this additive was omitted from the very beginning of the reaction, the resulting InAs@ZnSe systems exhibited either no PL emission or very low PLQY values.

2. Synthesis of TOA-AlH_3 and its Use in the One-Pot Synthesis of Amino-As-Based InAs and InAs@ZnSe QDs

We synthesized TOA-AlH_3 by dropwise addition of TOA into a mixture of $AlCl_3$ and $LiAlH_4$ in pentane, followed by filtration and removal of pentane (see Equation 1 and the Experimental Section for details).

$$AlCl_{3(s)} + 3LiAlH_{4(s)} + 4TOA_{(l)} \rightarrow 4\left(TOA - AlH_{3(l)}\right) + 3LiCl_{(s)} \quad (1)$$

The use of over stoichiometric amounts of $AlCl_3$ and $LiAlH_4$ led to the transformation of TOA into the TOA-AlH_3 adduct: the ^1H NMR spectrum of the product displayed peaks corresponding to TOA, shifted downfield to 2.60 ppm compared to pure TOA (2.47 ppm), due to the formation of a Lewis adduct between the nitrogen atom of TOA and the AlH_3 moiety (Figures S1 and S2, Supporting Information). Moreover, the product featured a broad peak at 4.39 ppm ascribable to the AlH_3 unit, consistent with similar compounds (Figures S1 and S2, Supporting Information).[52] The purity of the TOA-AlH_3 product was assessed via NMR analysis which returned a value of 91.7% (Figure S3, Supporting Information), and the reaction yield was calculated to be 84.9%. The TOA-AlH_3 reducing agent, compared to the more traditional reducing agents employed for the amino-As InAs QDs synthesis, including DMEA-AlH_3, DIBAL-H and HMTS, offers two main advantages: 1) the TOA released upon cleavage of the N—Al bond is a high-boiling compound (≈365 °C at 1 atm) unlike other commonly used reducing agents, which thermally decompose into low-boiling species; 2) TOA-AlH_3 can be dispersed/mixed with a high-boiling non-coordinating solvent, whereas commonly used reducing agents are commercially available in low-boiling solvents. ODE was selected as a suitable high-boiling non-coordinating solvent to dilute TOA-AlH_3 for two main reasons: i) to reduce TOA-AlH_3 high viscosity, thereby enabling smooth and consistent injection during the QD synthesis; ii) ODE is non-reactive toward TOA-AlH_3. This avoids unwanted side reactions that could degrade the precursor or alter its reducing power.

The new reducing agent was then employed in place of DMEA-AlH_3 in our established amino-As-based InAs QD one-pot synthesis protocol, which utilizes $ZnCl_2$ as an additive (see the Experimental Section for additional details).[46,48] In detail, we focused on adjusting the one-pot reaction conditions to achieve the largest possible QD size while maintaining a narrow size distribution. This was performed by fixing the amount of $InCl_3$ (0.2 mmol), $ZnCl_2$ (2 mmol), and amino-As (0.2 mmol) while systematically varying the reaction parameters, including the injection and reaction temperatures, as well as the relative amounts of TOA-AlH_3, Olam, non-coordinating solvent (i.e., ODE) and the reaction time.

Our experiments indicated that: i) the amount of TOA-AlH_3 should be equal to 0.8 mmol (4 equivalents with respect to As^{3+}), as lower amounts (i.e 0.6 mmol) produced QDs with broader size distribution (best ≈125meV), while higher amounts led to the formation of small InAs QDs with the presence of metallic In impurities (observed when using 1.0 and 1.5 mmol of TOA-AlH_3, see Section S4.1 and Figure S4, Supporting Information); ii) the injection and reaction temperatures should be maintained within the 240–280 °C range to promote QDs nucleation/growth, which occurs only when the injection temperature is at least 240 °C, and to prevent QD aggregation, which tends to occur at higher reaction temperatures (i.e., 300 °C, see the Section S4.2 and Figure S5, Supporting Information).

By employing 0.8 mmol of TOA-AlH_3 and setting the injection and reaction temperatures to 240 and 280 °C, respectively, the most significant effects on QD growth were observed when varying the relative amounts of ODE and Olam. Specifically, reducing the Olam amount from 5 to 2.5 mL while increasing the ODE volume from 0 to 7.5 mL resulted in InAs QDs with excitonic absorption peak tunable from roughly 750 to 1025 nm (**Figure 1a**) with HWHM values ranging from 100 meV up to more than 150meV (Figure 1b). This is in agreement with previous findings, which indicated that an optimal balance between the amount of Olam and the precursors concentration, the latter controlled by the volume of ODE, is one of the critical parameters to achieve larger InAs QDs, potentially with a narrow size distribution.[37,47]

By working with 5 mL of both Olam and ODE and a reaction time of 40 min (green curves in Figure 1a,b), we prepared InAs QDs (sample name InAs825) with a size of ≈2.9 nm (Figure S6a, Supporting Information) and an excitonic absorption peak at 825 nm with HWHM of 100 meV (Figure 1c and **Table 1**), similar to those obtained with DMEA-AlH_3 in our previous work (i.e., HWHM of 115 meV at 827 nm).[46,48] It is important to note that the HWHM values of the aliquots reported in Figure 1b were systematically larger than those of samples obtained under the same synthesis conditions and subjected to two cleaning steps (reported Table 1) similarly to what reported by Leemans et al.[37,44] Working with 3.3 mL of Olam and 6.7 mL of ODE (red curves in Figure 1a,b), it was possible to maximize the absorption peak position (935 nm) while maintaining a lower HWHM (≈85 meV, sample name InAs935, which is among the smallest values reported for amino-As based InAs QDs),[44,45,47,48,50] with a reaction time of ≈60 min (Figure 1d). Notably, the HWHM of InAs935 QDs was narrower than that of InAs QDs we previously obtained using DMEA–AlH_3 (>100 meV at the same wavelength).[48] The XRD patterns of both InAs825 and InAs935 QD samples were compatible with the cubic zinc-blende InAs phase (ICSD number 98-002-4518) with no presence of undesired secondary phases (Figure S6f, Supporting Information).

In order to boost the PL emission of both InAs QD samples, they were overcoated with a ZnSe shell by following an optimized in situ procedure previously developed by our group.[46] Such procedure consists in the addition of a 5.0 mL of a 0.8 M solution of $ZnCl_2$ in Olam (with a final Zn/In precursors ratio of 30:1) and 7.5 mL of a 1.0 M solution of Se in trioctylphosphine (TOP-Se, with a final Se/In precursors ratio of 37.5:1) to the crude InAs reaction solution at 300 °C for a time span of 180 min (see the experimental part for details). We anticipate here that this shelling procedure was employed for all the InAs@ZnSe systems discussed in this work.

The resulting InAs825@ZnSe (Figure S6b, Supporting Information) and InAs935@ZnSe (Figure 1f), core@shell QDs had a size of 9.0 ± 0.8 nm and 9.9 ± 0.7 nm, respectively, with a shell thickness of 7 and 6 monolayers (MLs), respectively (Table 1; Figure S6e, Table S2, Supporting Information), and featured a cubic zinc-blende crystal structure without any secondary phases

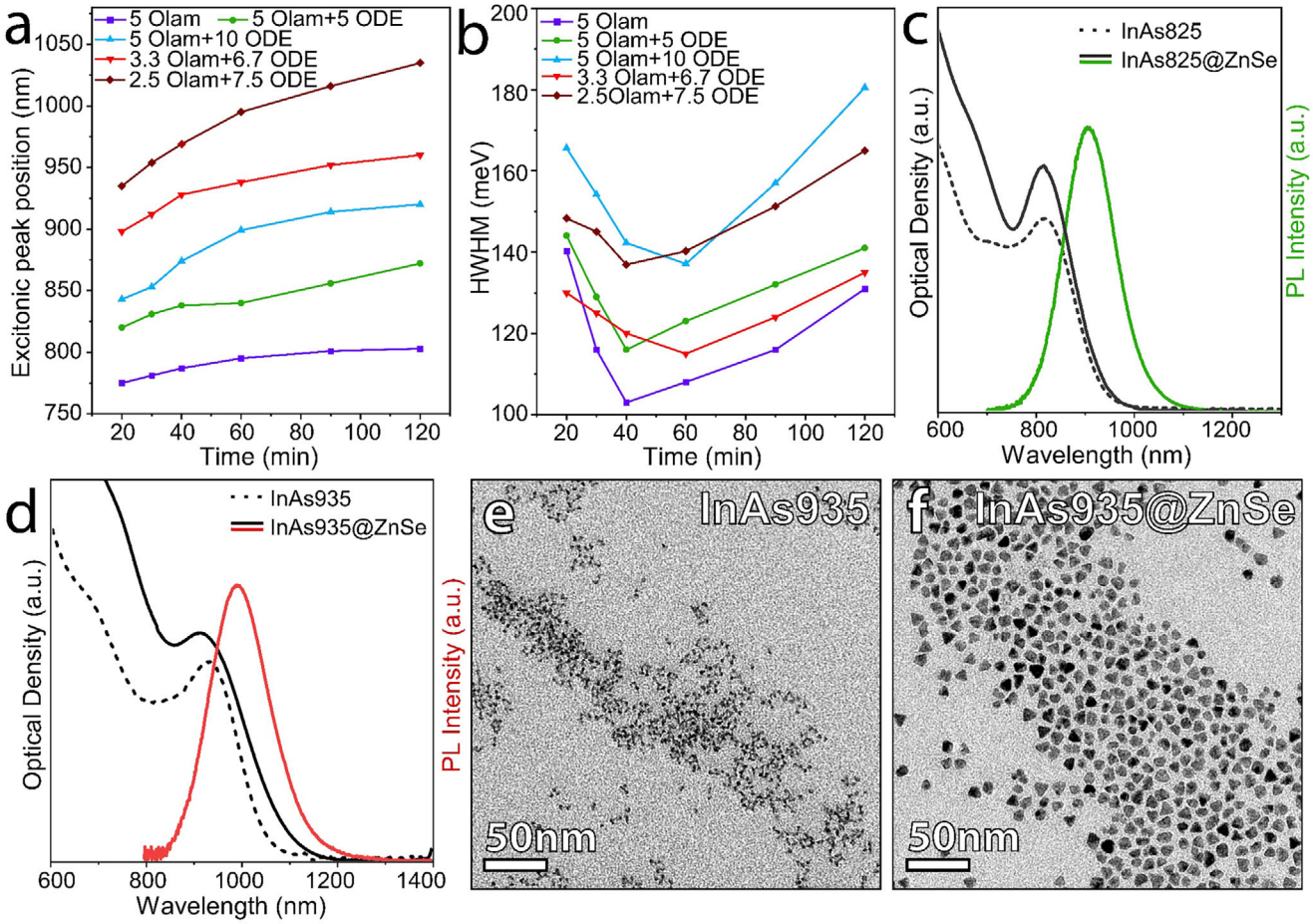

Figure 1. a) Variation of the excitonic peak position and b) the corresponding HWHM as a function of the reaction time when employing different Olam and ODE volumes (in mL) and working with 0.8 mmol of TOA-AlH_3 and setting the injection and reaction temperatures to 240 and 280 °C, respectively. Absorption and PL spectra of c) InAs825 and d) InAs935 QDs and the corresponding core@shell structures. Bright field (BF)-transmission electron microscopy (TEM) micrographs of e) InAs935 and f) InAs935@ZnSe QDs.

(Figure S6f, Supporting Information). The shell thickness was estimated from the QDs size, measured by TEM (see Figure 1e,f; Figure S6a,b, Supporting Information), combined with elemental analysis performed by inductively coupled plasma–optical emission spectroscopy (ICP-OES; Table S1, Supporting Information) and a structural model consisting of a tetrahedral InAs core of the desired size surrounded by a shell of variable thickness (Table S2, Supporting Information). It is worth highlighting here that, upon ZnSe shell growth, the In/As elemental ratio increased from ≈1.15 to ≈1.8 (Tables S1 and S2, Supporting Information) indicating the formation of an In-Zn-Se "interlayer", as already observed in our previous works. This interlayer is believed to reduce the strain between the InAs core and the ZnSe shell.[46,48] Remarkably, the InAs825@ZnSe QDs featured a PL peaked at 905 nm with PLQY as high as 75% (with a full width at half maximum, FWHM, of 190 meV, Figure 1c and Table 1), which compares favorably to the record efficiency reported for this kind of QDs (≈70% PLQY at ≈900 nm with a FWHM 220 meV and made with DMEA-AlH_3).[46] InAs935@ZnSe QDs exhibited emission at 1000 nm (FWHM of 185 meV) and a PLQY of 60%, a record

Table 1. Size, excitonic peak position, and corresponding HWHM of InAs825 and InAs935 QD samples. Size, number of ZnSe monolayers (MLs), and optical properties of the corresponding InAs@ZnSe core@shell QDs.

InAs			InAs@ZnSe Core@shell					
Size [nm]	Excitonic peak [nm]	HWHM [meV]	Size [nm]	ZnSe MLs	PL Peak [nm]	PLQY [%]	FWHM [meV]	Avg. Lifetime [ns]
2.9 ± 0.3	825	100	9.0 ± 0.8	7	905	75	190	55
3.7 ± 0.4	935	85	9.9 ± 0.7	6	1000	60	185	55

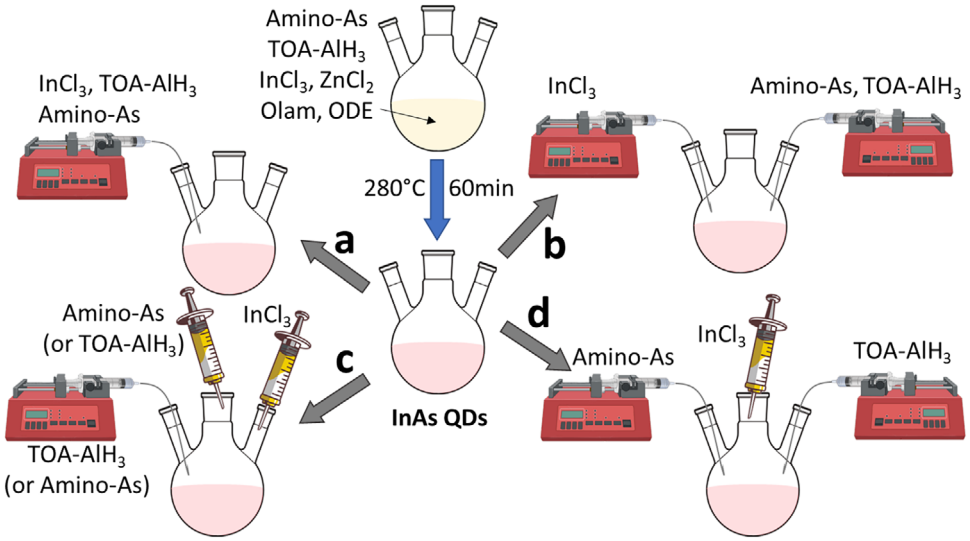

Figure 2. Schematic representation of the seeded growth procedures tested in the present work: a) simultaneous continuous injection of all the reactants; b) continuous co-injection of two different reactant solutions; c) addition of two reactants followed by continuous injection of the third; d) addition of $InCl_3$ followed by continuous co-injection of amino-As and TOA-AlH_3.

value for amino-As-based InAs QDs at this wavelength (Figure 1d and Table 1).

Overall, these results demonstrate the effectiveness of TOA-AlH_3 in the one-pot synthesis of amino-As based InAs QDs. Moreover, it is worth highlighting that in this set of experiments the injection of the TOA-AlH_3 solution into the hot precursors mixture resulted in a more stable reaction environment compared to that achieved with DMEA-AlH_3: i) the reaction temperature dropped by only ≈5 °C, significantly less than the 20–40 °C drop observed under analogous reaction conditions with DMEA-AlH_3; ii) no boiling burst occurred, unlike with DMEA-AlH_3 (see Movie S1, Supporting Information).

3. Enlarging InAs QDs through Seeded Growth Approaches

As shown in the previous section, the variation of the one-pot synthesis parameters did not enable the growth of InAs QDs with excitonic absorption peaks above 1000 nm while maintaining at the same time narrow excitonic absorption features. Therefore, to obtain larger QDs with control over their size distribution, we employed a different strategy, consisting in a seeded growth approach. In practice, we introduced additional In and As precursors into the crude InAs QD reaction mixture after they had reached a size of 3.7 nm (i.e., corresponding to an excitonic absorption peak position at ≈935 nm) (**Figure 2**). To this aim, we tested different operative methods, all discussed in detail in the Supporting Information (see Section S6 and Figures S7–S9, Supporting Information) and schematically depicted in Figure 2a–c. Most of these routes had issues, such as: i) the homonucleation of new InAs QDs; ii) the uncontrolled growth of the "seed" InAs QDs; iii) QD precipitation; iv) precursor solutions that were difficult to inject. The only successful strategy consisted in the direct addition of the required amount of $InCl_3$ to the "seed" InAs QD crude reaction mixture, followed by continuous co-injection of the TOA-AlH_3 and amino-As solutions (Figure 2d).

This successful strategy was then optimized by systematically varying the injection temperature (corresponding to the reaction temperature in this approach), and injection rates of both amino-As and TOA-AlH_3 solutions. The main results of this study were: i) the TOA-AlH_3 injection rate had to be twice that of amino-As in order to avoid the aggregation/precipitation of the QDs (Figure S10, Supporting Information); ii) an amino-As injection rate equal or slower than 0.005 mmol min^{-1} (corresponding to a TOA-AlH_3 rate of ≤0.01 mmol min^{-1} as per point i)) was essential to grow InAs QDs while minimizing the size distribution broadening (Figure S11, Supporting Information); iii) injection temperatures higher than 240 °C or lower than 220 °C resulted in the precipitation of the QDs (Figure S12, Supporting Information).

Under the best reaction conditions (i.e., an injection temperature of 240 °C and amino-As and TOA-AlH_3 injection rates of 0.005 and 0.01 mmol min^{-1}, respectively) it was possible to grow InAs QDs with sizes ranging from 4.6 to 6.3 nm (**Figure 3**a–d, **Table 2**; Figures S13a–d and S14a–d, Supporting Information). Correspondingly, the excitonic absorption peaks could be tuned from 1090 to 1340 nm (the samples were named accordingly InAs1090, InAs1170, InAs1250, and InAs1340) with HWHM values in the 92–99meV range (Figure 3i–l and Table 2), with no need to perform a size selection. Such HWHM values are comparable to the best values reported so far for amino-As-based InAs QDs, namely ≈95meV at 1380 nm and 90meV at 1420 nm.[49,50]

This was achieved by sequentially increasing the amounts of precursors used in the seeded growth approach from 2 to 7 equivalents, relative to those used in the initial one-pot synthesis of InAs QDs (see the Experimental Section for details). The XRD patterns of these samples indicated the absence of secondary phases, such as metallic In or In- or As-oxides, and the presence of the expected cubic zinc-blende InAs phase only (Figure S15a, Supporting Information).

The InAs QDs obtained via the seeded growth approach were subsequently overcoated with a ZnSe shell. BF-TEM analysis

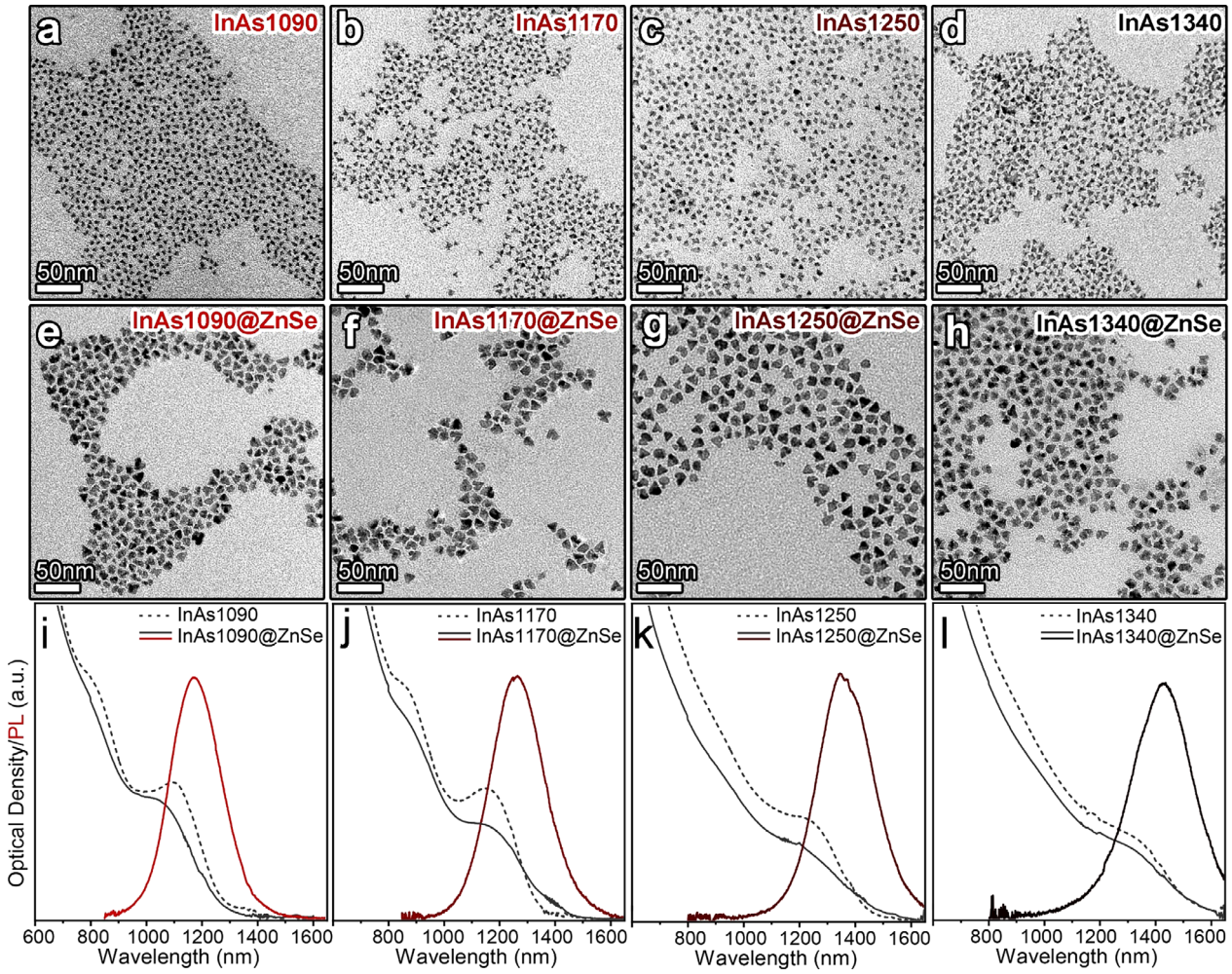

Figure 3. BF-TEM micrographs of a) InAs1090, b) InAs1170, c) InAs1250, and d) InAs1340 QDs, and e–h) the corresponding InAs@ZnSe core@shell structures. i–l) Absorption spectra (dotted lines) of the InAs QD samples, along with those of the corresponding core@shell structures (black lines) and their PL spectra (various shades of red in panels i–l).

confirmed the effective growth of the ZnSe shell, with the final InAs@ZnSe core@shell QDs having a ZnSe shell thickness of 6–8 MLs. (Figure 3e–h, Table 2; Figure S16a–d, Supporting Information). Additionally, XRD analyses confirmed the crystalline structure of the InAs@ZnSe core–shell QDs, which closely matched the ZnSe phase (ICSD 98-007-7092), with weak diffraction features from InAs, more intense in case of larger core sizes, and no presence of undesired secondary phases (Figure S15b, Supporting Information). Interestingly, the In/As elemental ratio was observed to increase upon the growth of the ZnSe shell (Tables S1 and S2, Supporting Information), suggesting the formation of an In-Zn-Se "interlayer" also in these larger QD systems.

InAs@ZnSe QDs featured PLQYs as high as 46% (1160 nm), 38% (1250 nm), 32% (1335 nm), and 23% (1430 nm), which are record values for these systems, achieved by optimizing the ZnSe

Table 2. Size, excitonic peak position, and HWHM of InAs QDs obtained via seeded growth. Size, number of ZnSe monolayers, and optical properties of the resulting InAs@ZnSe core@shell QDs.

InAs			InAs@ZnSe Core@shell					
Size [nm]	Abs. peak [nm]	HWHM [meV]	Size [nm]	ZnSe MLs	PL peak [nm]	PLQY [%]	FWHM [meV]	PL lifetime [ns]
4.6 ± 0.4	1090	99	10.2 ± 0.9	6	1160	46	191	67
5.2 ± 0.5	1170	97	11.8 ± 0.9	6	1250	38	177	78
5.7 ± 0.5	1250	98	12.1 ± 1.0	6–7	1335	32	158	86
6.3 ± 0.7	1340	92	12.5 ± 1.1	8	1430	23	154	95

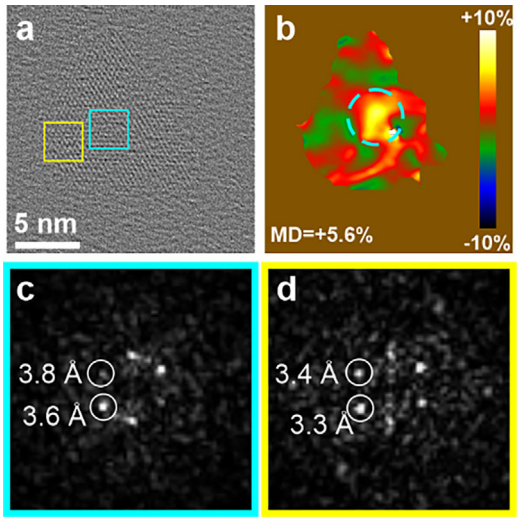

Figure 4. a) Average background subtraction-filtered HRTEM image of an InAs@ZnSe QD of the InAs1250@ZnSe sample and b) the corresponding mean dilation (MD) map computed by the PPA method, with the core region enclosed in the cyan circle. The MD reported in the panel is the average mean dilation within the core area compared to the shell. c,d) Fast Fourier transformations of areas enclosed in the (cyan) core and (yellow) shell areas of a), both matching with [111] direction of zinc-blende structures.

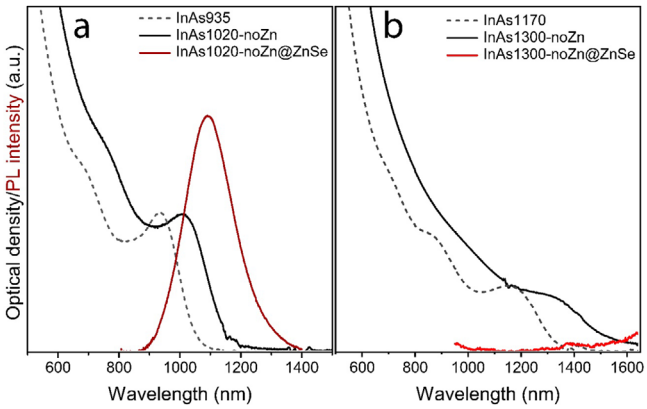

Figure 5. a) Absorption curve (black line) of InAs QDs synthesized without $ZnCl_2$ via the one-pot procedure, along with the PL spectrum (dark red line) of the corresponding QDs after ZnSe shelling. b) Absorption spectrum of InAs QDs synthesized without $ZnCl_2$ via seeded growth approach using three equivalents of added precursors (black line), together with the PL spectrum (red line) of the resulting InAs@ZnSe QDs. The absorption spectra of InAs935 and InAs1170 QD samples are also included in panels a) and b), respectively (gray dotted lines).

shell growth time for each core size (Figure 3i–l, Table 2; Figure S17b, Supporting Information). The average PL lifetime (Table 2; Figure S17c, Supporting Information) was observed to increase with increasing InAs core size, an effect that can be attributed to reduced carrier confinement in larger InAs QDs, leading to reduced radiative rates.[53–55]

High resolution (HR) TEM analyses of InAs@ZnSe QDs, chosen from the InAs1250@ZnSe sample, indicated that the majority of such core@shell structures are monocrystalline, most of them featuring a slightly truncated tetrahedral shape and composed of an InAs core surrounded by an epitaxial ZnSe shell (**Figure 4**). Tetrahedral QDs, as the one in Figure 4a, lie with one of the truncated triangular facets on the support carbon film parallel to the [111] direction of the common zinc-blende structure (Figure 4c,d). Strain analysis performed via peak pair analysis (PPA, see the Experimental Section for details) on the QD in Figure 4 revealed that the zinc-blende structure in the shell is characterized by lattice parameters 5.6% smaller than those of the core region (Figure 4b), a bit lower than what expected from the bulk values of the two different materials. PPA analysis performed on different QDs indicated that some InAs@ZnSe QDs feature a decentered InAs core (Figure S18, Supporting Information), which can be explained by a partially anisotropic ZnSe shell growth in these core@shell structures.

We would like to emphasize that amino-As-based InAs@ZnSe core@shell structures with efficient emission above 1000 nm have not been reported to date. This highlights the efficacy of our new reducing agent, TOA-AlH_3, which was crucial to achieve these results. Indeed, reducing agents dispersed in low-boiling-point solvents or those with a low boiling point themselves, such as DMEA-AlH_3, were observed to cause excessive boiling of the reaction mixture under analogous conditions, leading to unstable reaction conditions (see Movie S4, Supporting Information).

4. Role of $ZnCl_2$

All the reaction schemes illustrated so far included the use of $ZnCl_2$ in the synthesis of InAs QDs. This additive was employed in the one-pot synthesis of InAs QDs (with a Zn/In precursors ratio of 10/1) and remained in the crude reaction solution in the whole seeded-growth procedure. Under the optimized reaction conditions described above, the absence of $ZnCl_2$ (details in Section S10, Supporting Information) led to two main differences:

i) the formation of larger InAs QDs. For example, at the end of the one-pot synthesis, InAs QDs with an absorption peak at 1020 nm were obtained (named InAs1020-noZn), compared to 935 nm when $ZnCl_2$ was used (i.e., sample InAs935, **Figures 5a** and 1d). Similarly, after employing three equivalents of precursors in the seeded growth approach, the InAs QDs exhibited an excitonic peak at 1300 nm (named InAs1300-noZn), whereas those synthesized with $ZnCl_2$ showed a peak at 1170 nm (i.e., sample InAs1170, Figures 5b and 3j).

ii) Upon ZnSe shelling, InAs QDs synthesized without $ZnCl_2$ had either very low PLQY values (10% with PL at 1100 nm, sample InAs1020-noZn@ZnSe, Figure 5a; Table S4, Supporting Information) or no PL emission (sample InAs1300-noZn@ZnSe, Figure 5b; see also Table S5, Supporting Information).

These results not only further reinforce our previous findings, which identified $ZnCl_2$ as an indispensable additive to prepare InAs@ZnSe QDs with high PLQY, but also highlight a key advantage of our new reducing agent. In fact, alternative synthesis methods that employ different reducing agents, such as amino-P[37] or HMTS,[49] are incompatible for the preparation of InAs

QDs in the presence of $ZnCl_2$. Specifically, in the case of amino-P, $ZnCl_2$ was observed to induce QD aggregation, while the synthesis using HMTS delivered InAs QDs with anisotropic shapes (e.g., tetrapods); for these reasons, the additive was excluded from the synthesis in both studies.

5. Conclusion

We have reported an amino-As-based synthesis of InAs@ZnSe QDs that can emit up to 1400 nm with high PL efficiency. This result was achieved using TOA-AlH_3 as a reducing agent, which was synthesized in our lab and employed not only for the synthesis of InAs QDs through a hot-injection procedure, but also for their subsequent growth in situ via a seeded-growth approach. TOA-AlH_3 can be dispersed in high-boiling-point solvents and has a high boiling point itself, enabling precise control over reaction conditions even during continuous addition in the seeded growth. This is in stark contrast to traditional reducing agents used in the amino-As route, which have a low boiling point and are dispersed in low-boiling-point solvents (e.g., DMEA-AlH_3, DIBAL-H, etc.). Moreover, TOA-AlH_3 is compatible with the $ZnCl_2$ additive in the InAs QDs reaction environment, a condition found to be essential to synthesize InAs@ZnSe core@shell QDs with efficient PL.

As for the seeded growth approach, we found that $InCl_3$, amino-As, and TOA-AlH_3 must be added to the crude reaction solution containing "seed" InAs QDs in a specific order to prevent precipitation or uncontrolled growth. Specifically, the optimal strategy for growing InAs QDs was to first add $InCl_3$, followed by the continuous co-injection of amino-As and TOA-AlH_3 at different rates. In conclusion, this work further highlights the potential of amino-As-based InAs QDs for the development of future IR-based technologies.

6. Experimental Section

Chemicals: Indium(III) chloride ($InCl_3$, 99.999%, Sigma–Aldrich), zinc(II) chloride ($ZnCl_2$, 99.999%, Sigma–Aldrich), lithium aluminum hydride ($LiAlH_4$, 95%, Sigma–Aldrich), aluminum(III) chloride ($AlCl_3$, 99.999%, Sigma–Aldrich), tris(dimethylamino)arsine (amino-As, 99%, Strem), alane N,N-dimethylethylamine complex solution (DMEA-AlH_3, 0.5 M solution in toluene, Sigma–Aldrich), oleylamine (Olam, 98%, Sigma–Aldrich), 1-octadecene (ODE, 90%, Sigma–Aldrich), selenium powder (Se, 99.99%, Strem), tri-n-octylphosphine (TOP, 97%, Strem), trioctylamine (TOA, 98%, Sigma–Aldrich), toluene (anhydrous, 99.8%, Sigma–Aldrich), pentane (anhydrous, 99%, Sigma–Aldrich), tetrachloroethylene (TCE, anhydrous, 99%, Sigma–Aldrich), ethanol (anhydrous, 99.8%, Sigma–Aldrich). All the chemicals were used without further purification. Olam, TOA, and ODE were degassed at 120 °C under vacuum for 1.5 h before use.

Synthesis of the TOA-AlH_3 Adduct: In a 250 mL flat-bottom Florence flask, 3.7 g (28.3 mmol) of $AlCl_3$, 3.6 g (94.9 mmol) of $LiAlH_4$, and 100 mL of pentane were added. 40.6 mL (93 mmol) of TOA was then added dropwise to the reaction mixture to prevent a sudden rise in temperature. The flask was sealed to minimize solvent evaporation and stirred overnight. Upon completion of the reaction, the mixture was filtered using Whatman filter paper to remove unreacted residues. The filtrate was then degassed under vacuum to remove pentane, yielding pure TOA-AlH_3. The reducing agent was stored under an inert atmosphere in a glovebox at low temperatures (−20 °C) for subsequent use. Prior to injection into the reaction mixture, TOA-AlH_3 was mixed with a high-boiling solvent such as ODE to ensure compatibility with high-temperature reaction conditions.

Preparation of $InCl_3$-Olam (0.2 M) Precursor: 0.88 g (4 mmol) of $InCl_3$ and 20 mL of Olam were taken in a three-neck flask. The mixture was degassed at 120 °C for 30 min, then heated up to 250 °C for an additional 30 min until the solution became clear. Afterward, the solution was cooled down to room temperature and stored under inert atmosphere for use in subsequent synthesis.

Preparation of Amino-As Precursor Solution: Inside a N_2 filled glovebox, 0.2 mmol of amino-As was dissolved in 0.5 mL of degassed Olam (that is 0.4 M) in a vial at 60 °C for 5 min, until no further bubbles were observed. The amino-As solutions in Olam employed for the seeded growth approaches were prepared with the same procedure with the only difference being the molarity that was set to 0.1 M.

Preparation of 0.8 M $ZnCl_2$-Olam Precursor: In a N_2 filled glovebox, 8 mmol of $ZnCl_2$ was dissolved in 10 mL of OLAM in a 20 mL glass vial by heating the mixture up to 250 °C under constant stirring for 30 min. $ZnCl_2$-Olam solidifies at room temperature, therefore the solution must be heated up to 100 °C before use.

Preparation of 1.0 M TOP-Se Precursor: In a N_2 filled glovebox, 20 mmol of Se powder was mixed with 20 mL of TOP in a 40 mL glass vial and heated at 120 °C under stirring for 30 min. The resulting solution was cooled down to room temperature.

One-Pot Hot-Injection Synthesis of InAs@ZnSe core@shell QDs Emitting at 905 or 1000nm: In a typical synthesis, 0.2 mmol of $InCl_3$ and 2 mmol of $ZnCl_2$ were weighed into a 50 mL three-neck round-bottom flask. Varying amounts of Olam (5, 3.3, or 2.5 mL) and ODE (0, 5, 6.7, or 7.5 mL) were added to the flask. InAs825 was synthesized using 5 mL of Olam and 5 mL of ODE, while InAs935 was synthesized using 3.3 mL of Olam and 6.7 mL of ODE. The mixture was degassed at room temperature for 15 min, followed by degassing at 120 °C for 1 h under vacuum. The temperature was then raised to 240 °C under a nitrogen atmosphere, and the As precursor was injected at this temperature. Upon injection, the reaction temperature momentarily dropped by ≈5 °C and recovered to 240 °C within ≈20 s. Subsequently, 0.8 mmol of TOA-AlH_3 dissolved in 5 mL of ODE was swiftly injected into the reaction mixture at 240 °C, and the temperature was increased to 280 °C at a rate of ≈5 °C min^{-1}. The reaction was allowed to proceed for 60 min before quenching by removing the heating mantle and cooling the mixture to 90 °C.

For the ZnSe shell growth, 5.0 mL of 0.8 M $ZnCl_2$-OLAM and 7.5 mL of 0.1 M TOP-Se solutions were injected into the crude reaction mixture at 90 °C, followed by heating to 300 °C under an inert atmosphere. After 120 min, the reaction was quenched by removing the heating mantle, followed by the addition of 5 mL of toluene. The mixture was centrifuged at 4000 rpm to remove aggregates and agglomerates. The resulting supernatant was collected, and the QDs were precipitated by adding ethanol, followed by centrifugation at 3000 rpm. The QDs underwent two additional washing steps before being dispersed in TCE for further characterization. All washing steps were performed inside a nitrogen-filled glovebox.

Synthesis of InAs@ZnSe core@shell QDs via the Seeded Growth Approach: InAs QDs were synthesized following the procedure employed to produce InAs935 QDs. After 60 min, upon completion of InAs QDs synthesis, the reaction temperature was lowered to 240 °C. At this stage, 2, 3, 5, or 7 mL of 0.2 M $InCl_3$-Olam solution was injected into the crude reaction mixture in order to grow InAs QDs larger (details in table below). Immediately afterward, 4, 6, 10, and 14 mL of 0.1 M amino-As solution along with equal volumes of 0.2 M TOA-AlH_3 solution, were loaded into two syringes (20 mm in diameter) and connected to two syringe pumps for continuous injection (details in **Table 3**).

The continuous injection of the two precursors was performed at 240 °C with a rate of 0.05 mL min^{-1} (which is 0.005 and 0.01 mmol min^{-1} with respect to amino-As and TOA-AlH_3, respectively). After both precursors were completely injected, the heating mantle was removed, and the reaction mixture was cooled down to room temperature using compressed air. The samples were washed by addition of 10 mL of toluene followed by centrifugation at 4000 rpm to remove undesired byproducts and aggregates. The supernatant was collected and washed via the addition of ethanol followed by centrifugation at 4000 rpm. The purified InAs QDs

Table 3. Injection amounts (in mmol) of additional precursors ($InCl_3$, amino-As, and TOA-AlH_3) and continuous injection durations used in the seeded growth of InAs935 QDs to obtain larger QDs with red-shifted excitonic absorption features.

Excitonic peak position [nm]	Equivalents of precursors added	Amount of In precursor [mmol]	Amount of As precursor [mmol]	Amount of TOA-AlH_3 [mmol]	Cont. Inj. duration [min]
1090	2	0.4	0.4	0.8	80
1170	3	0.6	0.6	1.2	120
1250	5	1.0	1.0	2.0	200
1340	7	1.4	1.4	2.8	280

were dispersed in 10 mL of Olam and transferred to a 50 mL three-neck flask under an inert atmosphere. The mixture was degassed at room temperature for 30 min to remove residual toluene or ethanol. Subsequently, the temperature was raised to 90 °C under N_2 atmosphere. At this stage, 7.5 mL of 0.8 M of $ZnCl_2$-Olam and 6.0 mL of 1.0 M TOP-Se solutions were injected into the reaction mixture and the corresponding mixture was heated up to 300 °C under N_2 atmosphere. After 120 min, the reaction was quenched by removing the heating mantle. 5 mL of toluene was added to the reaction mixture, and the solution was centrifuged at 4000 rpm to remove any unreacted impurities. The supernatant was further washed twice with toluene and ethanol, followed by centrifugation at 3000 rpm. The purified InAs@ZnSe QDs were dispersed in TCE and stored under an inert atmosphere for further characterization.

X-Ray Diffraction (XRD): XRD patterns were acquired using a PANalytical Empyrean X-ray diffractometer equipped with a 1.8 kW Cu Kα ceramic X-ray tube and a PIXcel3D 2 × 2 area detector, operating at 45 kV and 40 mA. Specimens for XRD measurements were prepared by depositing a concentrated QD solution onto a silicon zero-diffraction single-crystal substrate. The diffraction patterns were recorded under ambient conditions using a parallel beam geometry in symmetric reflection mode. XRD data analysis was performed using HighScore 4.1 software (PANalytical).

Transmission Electron Microscopy (TEM): Diluted QDs solutions were drop-cast onto copper TEM grids with an ultrathin carbon film. Overview BF-TEM images were acquired on a JEOL JEM-1400Plus microscope with a thermionic gun (LaB_6) operated at an acceleration voltage of 120 kV. HRTEM images were acquired by an image-Cs-corrected JEM-2200FS, operated at 200 kV, using a direct-electron-detection camera (Gatan K2 Summit) at a comparatively low dose rate ($\approx 30\ e^-\ (s \bullet Å^2)^{-1}$) so as to minimize carbon contamination. The images presented here were extracted from original $(280\ nm)^2$ frames, obtained by cross-correlated sum of 40 frames, each obtained with 0.3 s exposure. The HRTEM images shown here were Fourier-filtered, using an average background subtraction filter (ABSF),[56] to minimize the contribution to the contrast from the amorphous component. The peak pair analysis (PPA)[57] method was used to compute the mean dilation map from the HRTEM image of individual core–shell particles, with the aim of identifying the position of the InAs core by mapping the lattice parameters within the core@shell QDs.

Optical Characterization: The absorption spectra were recorded using a Varian Cary 5000 UV–vis–NIR spectrophotometer. The samples were prepared by diluting the QDs solution in 3 mL of TCE in 1 cm path length quartz cuvettes, sealed with airtight screw caps, inside a N_2 filled glovebox. Aliquots were taken directly from the reaction mixture using a glass syringe, diluted with toluene, and their absorption was measured under ambient conditions. Steady-state and time-resolved PL measurements were conducted using an Edinburgh Instruments FLS900 fluorescence spectrometer. Steady-state PL excitation was performed with a xenon lamp and a monochromator, while time-resolved PL was measured using a time-correlated single-photon counting (TCSPC) unit coupled with an Edinburgh Instruments EPL-510 pulsed laser diode (λ_{ex} = 508.2 nm, pulse width = 177.0 ps). PLQY measurements were carried out using the same spectrometer equipped with an integrating sphere, with excitation at 700 nm from the Xe lamp output. All QD solutions were diluted to an optical density of ≈0.1 at the excitation wavelength.

Supporting Information

Supporting Information is available from the Wiley Online Library or from the author.

Acknowledgements

The authors acknowledge Dorwal Marchelli for the support in the optical analyses and Habibul Arfin and Francesco De Donato for helping with the synthesis of TOA-AlH_3. The authors acknowledge funding from the Project IEMAP (Italian Energy Materials Acceleration Platform) within the Italian Research Program ENEA-MASE (Ministero dell'Ambiente e della Sicurezza Energetica) 2021-2024 "Mission Innovation" (agreement 21A033302 GU n. 133/5-6-2021).

Open access publishing facilitated by Istituto Italiano di Tecnologia, as part of the Wiley - CRUI-CARE agreement.

Conflict of Interest

The authors declare no conflict of interest.

Data Availability Statement

Data available by the corresponding author upon reasonable request.

Keywords

III-V semiconductors, core@shell, indium arsenide, infrared, quantum dots

Received: May 14, 2025
Revised: August 4, 2025
Published online:

[1] T. Müller, J. Skiba-Szymanska, A. B. Krysa, J. Huwer, M. Felle, M. Anderson, R. M. Stevenson, J. Heffernan, D. A. Ritchie, A. J. Shields, *Nat. Commun.* **2018**, *9*, 862.
[2] J. Chen, S. Zheng, D. Jia, W. Liu, A. Andruszkiewicz, C. Qin, M. Yu, J. Liu, E. M. J. Johansson, X. Zhang, *ACS Energy Lett.* **2021**, *6*, 1970.
[3] S. Liu, K. Xiong, K. Wang, G. Liang, M.-Y. Li, H. Tang, X. Yang, Z. Huang, L. Lian, M. Tan, K. Wang, L. Gao, H. Song, D. Zhang, J. Gao, X. Lan, J. Tang, J. Zhang, *ACS Nano* **2021**, *15*, 3376.
[4] J. H. Song, H. Choi, H. T. Pham, S. Jeong, *Nat. Commun.* **2018**, *9*, 4267.
[5] P. Geiregat, A. J. Houtepen, L. K. Sagar, I. Infante, F. Zapata, V. Grigel, G. Allan, C. Delerue, D. Van Thourhout, Z. Hens, *Nat. Mater.* **2018**, *17*, 35.

[6] S. Christodoulou, I. Ramiro, A. Othonos, A. Figueroba, M. Dalmases, O. Özdemir, S. Pradhan, G. Itskos, G. Konstantatos, *Nano Lett.* **2020**, *20*, 5909.
[7] P. M. Allen, W. Liu, V. P. Chauhan, J. Lee, A. Y. Ting, D. Fukumura, R. K. Jain, M. G. Bawendi, *J. Am. Chem. Soc.* **2010**, *132*, 470.
[8] D. Franke, D. K. Harris, O. Chen, O. T. Bruns, J. A. Carr, M. W. B. Wilson, M. G. Bawendi, *Nat. Commun.* **2016**, *7*, 12749.
[9] K. Takemoto, M. Takatsu, S. Hirose, N. Yokoyama, Y. Sakuma, T. Usuki, T. Miyazawa, Y. Arakawa, *J. Appl. Phys.* **2007**, *101*, 081720.
[10] S. Pradhan, F. Di Stasio, Y. Bi, S. Gupta, S. Christodoulou, A. Stavrinadis, G. Konstantatos, *Nat. Nanotechnol.* **2019**, *14*, 72.
[11] S. Goossens, G. Navickaite, C. Monasterio, S. Gupta, J. J. Piqueras, R. Pérez, G. Burwell, I. Nikitskiy, T. Lasanta, T. Galán, E. Puma, A. Centeno, A. Pesquera, A. Zurutuza, G. Konstantatos, F. Koppens, *Nat. Photonics* **2017**, *11*, 366.
[12] M. Vasilopoulou, A. Fakharuddin, F. P. García de Arquer, D. G. Georgiadou, H. Kim, A. R. b. Mohd Yusoff, F. Gao, M. K. Nazeeruddin, H. J. Bolink, E. H. Sargent, *Nat. Photonics* **2021**, *15*, 656.
[13] S. Kumar, S. Pradhan, *Adv. Opt. Mater.* **2024**, *12*, 2400993.
[14] M. De Franco, D. Zhu, A. Asaithambi, M. Prato, E. Charalampous, S. Christodoulou, I. Kriegel, L. De Trizio, L. Manna, H. Bahmani Jalali, F. Di Stasio, *ACS Energy Lett.* **2022**, *7*, 3788.
[15] H. Roshan, D. Zhu, D. Piccinotti, J. Dai, M. De Franco, M. Barelli, M. Prato, L. De Trizio, L. Manna, F. Di Stasio, *Adv. Sci.* **2024**, *11*, 2400734.
[16] S. Keuleyan, E. Lhuillier, P. Guyot-Sionnest, *J. Am. Chem. Soc.* **2011**, *133*, 16422.
[17] A. K. Bansal, F. Antolini, S. Zhang, L. Stroea, L. Ortolani, M. Lanzi, E. Serra, S. Allard, U. Scherf, I. D. W. Samuel, *J. Phys. Chem. C* **2016**, *120*, 1871.
[18] S. A. McDonald, G. Konstantatos, S. Zhang, P. W. Cyr, E. J. D. Klem, L. Levina, E. H. Sargent, *Nat. Mater.* **2005**, *4*, 138.
[19] J. M. Pietryga, R. D. Schaller, D. Werder, M. H. Stewart, V. I. Klimov, J. A. Hollingsworth, *J. Am. Chem. Soc.* **2004**, *126*, 11752.
[20] J. Schubert, E. J. Riley, S. A. Tyler, *J. Toxicol. Environ. Health* **1978**, *4*, 763.
[21] J. Sobhanan, P. Jones, R. Kohara, S. Sugino, M. Vacha, C. Subrahmanyam, Y. Takano, F. Lacy, V. Biju, *Nanoscale* **2020**, *12*, 22049.
[22] European Union, Directive 2011/65/EU of the European Parliament and of the Council of 8 June 2011 on the Restriction of the Use of Certain Hazardous Substances in Electrical and Electronic Equipment (consolidated version 2025). EUR-Lex, https://eur-lex.europa.eu/legal-content/EN/TXT/?uri=CELEX:02011L0065-20250101.
[23] E. George, M. Pecht, *Microelectron. Reliab.* **2016**, *65*, 1.
[24] C.-O. Gensch, Y. Baron, M. Blepp, O. Deubzer, in *Assistance to the Commission on Technological Socio-Economic and Cost-Benefit Assessment Related to Exemptions from the Substance Restrictions in Electrical and Electronic Equipment (RoHS Directive)*, Öko-Institut eV, Freiburg, Germany **2016**.
[25] Y. Ma, Y. Zhang, W. W. Yu, *J. Mater. Chem. C* **2019**, *7*, 13662.
[26] L. Yang, S. Zhang, B. Xu, J. Jiang, B. Cai, X. Lv, Y. Zou, Z. Fan, H. Yang, H. Zeng, *Nano Lett.* **2023**, *23*, 2443.
[27] W. J. Mir, T. Sheikh, S. Nematulloev, P. Maity, K. E. Yorov, A.-H. Emwas, M. N. Hedhili, M. S. Khan, M. Abulikemu, O. F. Mohammed, O. M. Bakr, *Small* **2024**, *20*, 2306535.
[28] L. Asor, J. Liu, S. Xiang, N. Tessler, A. I. Frenkel, U. Banin, *Adv. Mater.* **2023**, *35*, 2208332.
[29] D. Darwan, L. J. Lim, T. Wang, H. Wijaya, Z.-K. Tan, *Nano Lett.* **2021**, *21*, 5167.
[30] D. Franke, D. K. Harris, L. Xie, K. F. Jensen, M. G. Bawendi, *Angew. Chem.* **2015**, *127*, 14507.
[31] G. Schileo, G. Grancini, *J. Mater. Chem. C* **2021**, *9*, 67.
[32] D. Battaglia, X. Peng, *Nano Lett.* **2002**, *2*, 1027.
[33] S. Tamang, S. Lee, H. Choi, S. Jeong, *Chem. Mater.* **2016**, *28*, 8119.
[34] T. Kim, S. Park, S. Jeong, *Nat. Commun.* **2021**, *12*, 3013.
[35] H. B. Jalali, L. De Trizio, L. Manna, F. Di Stasio, *Chem. Soc. Rev.* **2022**, *51*, 9861.
[36] T. Sheikh, W. J. Mir, S. Nematulloev, P. Maity, K. E. Yorov, M. N. Hedhili, A.-H. Emwas, M. S. Khan, M. Abulikemu, O. F. Mohammed, O. M. Bakr, *ACS Nano* **2023**, *17*, 23094.
[37] J. Leemans, D. Respekta, J. Bai, S. Braeuer, F. Vanhaecke, Z. Hens, *ACS Nano* **2023**, *17*, 20002.
[38] M. Kim, J. Lee, J. Jung, D. Shin, J. Kim, E. Cho, Y. Xing, H. Jeong, S. Park, S. H. Oh, Y.-H. Kim, S. Jeong, *J. Am. Chem. Soc.* **2024**, *146*, 10251.
[39] Z. Liu, J. Llusar, H. H. Karakkal, D. Zhu, Y. P. Ivanov, M. Prato, G. Divitini, S. Brovelli, I. Infante, L. De Trizio, L. Manna, *Adv. Energy Mater.* **2024**, *14*, 2402246.
[40] R. L. Wells, C. G. Pitt, A. T. McPhail, A. P. Purdy, S. Shafieezad, R. B. Hallock, *Chem. Mater.* **1989**, *1*, 4.
[41] D. K. Harris, M. G. Bawendi, *J. Am. Chem. Soc.* **2012**, *134*, 20211.
[42] X. Peng, J. Wickham, A. P. Alivisatos, *J. Am. Chem. Soc.* **1998**, *120*, 5343.
[43] V. Srivastava, E. M. Janke, B. T. Diroll, R. D. Schaller, D. V. Talapin, *Chem. Mater.* **2016**, *28*, 6797.
[44] V. Grigel, D. Dupont, K. De Nolf, Z. Hens, M. D. Tessier, *J. Am. Chem. Soc.* **2016**, *138*, 13485.
[45] V. Srivastava, E. Dunietz, V. Kamysbayev, J. S. Anderson, D. V. Talapin, *Chem. Mater.* **2018**, *30*, 3623.
[46] D. Zhu, H. Bahmani Jalali, G. Saleh, F. Di Stasio, M. Prato, N. Polykarpou, A. Othonos, S. Christodoulou, Y. P. Ivanov, G. Divitini, I. Infante, L. De Trizio, L. Manna, *Adv. Mater.* **2023**, *35*, 2303621.
[47] Z. Liu, R. Pascazio, L. Goldoni, D. Maggioni, D. Zhu, Y. P. Ivanov, G. Divitini, J. L. Camarelles, H. B. Jalali, I. Infante, L. De Trizio, L. Manna, *J. Am. Chem. Soc.* **2023**, *145*, 18329.
[48] D. Zhu, F. Bellato, H. Bahmani Jalali, F. Di Stasio, M. Prato, Y. P. Ivanov, G. Divitini, I. Infante, L. De Trizio, L. Manna, *J. Am. Chem. Soc.* **2022**, *144*, 10515.
[49] M. S. Skorotetcky, W. J. Mir, T. Sheikh, K. E. Yorov, B. M. Saidzhonov, S. Daws, R. Zhou, M. N. Hedhili, M. Abulikemu, O. F. Mohammed, O. M. Bakr, *Adv. Mater.* **2024**, *37*, 2412105.
[50] M. Ginterseder, D. Franke, C. F. Perkinson, L. Wang, E. C. Hansen, M. G. Bawendi, *J. Am. Chem. Soc.* **2020**, *142*, 4088.
[51] L. K. Sagar, G. Bappi, A. Johnston, B. Chen, P. Todorović, L. Levina, M. I. Saidaminov, F. P. García de Arquer, D.-H. Nam, M.-J. Choi, S. Hoogland, O. Voznyy, E. H. Sargent, *Chem. Mater.* **2020**, *32*, 7703.
[52] T. D. Humphries, K. T. Munroe, A. Decken, G. S. McGrady, *Dalton Trans.* **2013**, *42*, 6965.
[53] J. M. An, A. Franceschetti, A. Zunger, *Nano Lett.* **2007**, *7*, 2129.
[54] H. Du, C. Chen, R. Krishnan, T. D. Krauss, J. M. Harbold, F. W. Wise, M. G. Thomas, J. Silcox, *Nano Lett.* **2002**, *2*, 1321.
[55] J. Hours, P. Senellart, E. Peter, A. Cavanna, J. Bloch, *Phys. Rev. B* **2005**, *71*, 161306.
[56] R. Kilaas, *J. Microsc.* **1998**, *190*, 45.
[57] P. L. Galindo, S. Kret, A. M. Sanchez, J.-Y. Laval, A. Yáñez, J. Pizarro, E. Guerrero, T. Ben, S. I. Molina, *Ultramicroscopy* **2007**, *107*, 1186.